ELSEVIER

Polymer 41 (2000) 4223–4231

polymer

In situ rehydration of perfluorosulphonate ion-exchange membrane studied by AFM

P.J. James[a,*], T.J. McMaster[a], J.M. Newton[b], M.J. Miles[a]

[a]*University of Bristol, H.H. Wills Physics Laboratory, Tyndall Avenue, Bristol BS8 1TL, UK*
[b]*National Power PLC, Harwell International Business Centre, Harwell, Didcot, OX11 0QA, UK*

Received 29 March 1999; received in revised form 30 July 1999; accepted 1 September 1999

Abstract

Nafion® is a commercially available perfluorosulphonate cation exchange membrane commonly used as a perm-selective separator in chlor-alkali electrolysers and as the electrolyte in solid polymer fuel cells. This usage arises because of its high mechanical, thermal and chemical stability coupled with its high conductivity and ionic selectivity, which depend strongly on the water content. The membrane was therefore studied in different states of hydration obtained by placing the membrane and atomic force microscope (AFM) in a specially constructed environmental chamber to control the humidity. Tapping mode phase imaging was successfully used to identify the hydrophobic and hydrophilic regions of Nafion. The images support a cluster model for the hydrophilic regions of Nafion at humidities of (9–34) ± 2%. The clusters have a range of sizes from 5 to 30 nm, significantly larger than the ~4 nm structures proposed from X-ray studies, which is probably due to the formation of cluster agglomerates. Phase images were interpreted semi-quantitatively in terms of energy loss, typically 3 kJ m^{-2}, and the number and size of energy dissipative features. The number of clusters decreased while the average cluster size increased with increasing humidity.

Keywords: Nafion; Perfluorinated ionomer membrane; Atomic force microscopy

1. Introduction

Nafion® is a commercially available perfluorosulphonate cation exchange membrane (CEM) manufactured by E I du Pont de Nemours & Co. Inc. It is commonly used as a perm-selective separator in chlor-alkali electrolysers [1,2] and as the electrolyte in solid polymer fuel cells (SPFC). Perfluorosulphonate cation exchange membranes are used in these applications because of their high ionic conductivity and their high mechanical, thermal and chemical stability. Structurally, Nafion consists of a hydrophobic tetrafluoroethylene (TFE) backbone with pendant side chains of perfluorinated vinyl ethers terminated by ion-exchange groups. The chemical structure of Nafion is shown in Fig. 1. The ion content can be varied by changing the ratio of the two components.

Other perfluoro-sulphonate cation exchange membranes with similar structures have also been developed by the Asahi Chemical Company (Aciplex®) and the Asahi Glass Company (Flemion®). The Dow Chemical Company also developed a material with a shorter side-chain than those of Nafion and the other perfluoro-sulphonates [3].

The ionic conductivity in perfluor-sulphonate membranes is important since it should be as high as possible to minimize ohmic losses in chlor-alkali electrolysers and to maintain high output power densities in fuel cell applications. The membrane conductivity is strongly influenced by the water content [4]. Water management is also an important problem for efficient SPFC operation to avoid flooding of the gas diffusion electrodes. A number of factors affect the water content including the cation form, ion-exchange capacity of the membrane and equivalent weight (EW). The ion content is usually expressed in terms of the equivalent weight of the polymer. The equivalent weight is defined as the weight of dry polymer in grams containing one mole of exchange sites. The desired equivalent weight is achieved by varying the ratio of vinyl ether monomer to TFE. The useful range of equivalent weights is from the 600–1500 g mol^{-1}, between the solubility and percolation limits. The industrial applications of Nafion have prompted considerable research effort summarised by Eisenberg and Yeager [5] in 1982 and more recently by Tant et al. [3] in 1997.

Perfluoro-sulphanate polymers typically have ordered structures where the hydrophillic end groups aggregate within the hydrophobic matrix composed of the

* Corresponding author. Tel.: +44-0117-9288747; fax: +44-0117-9255624.

0032-3861/00/$ - see front matter
PII: S0032-3861(99)00641-2

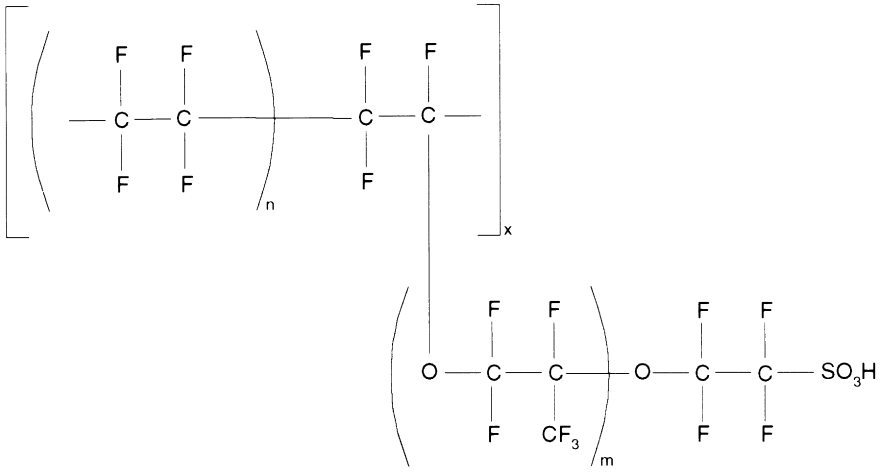

$$C_{(2n+3m+4)}F_{(4n+6m+7)}O_{(m+4)}SH$$

Fig. 1. The structural repeat of Nafion.

fluorocarbon backbone of the polymer. Many models have been proposed to describe the structural organisation of the perfluoro-sulphonate polymers. They can be divided into two groups: the first group of models suggests that all the sulphonate groups are in an aqueous phase, consisting of well-defined clusters and channels. The other group of models postulates on the presence of an intermediate region between the fluorocarbon backbone and the aqueous phase. The intermediate region would contain the pendant side chain, the sulphonate group and some fluorocarbon backbone.

The majority of studies on Nafion to date have been carried out using X-ray diffraction [6–9], electron microscopy [10,11] and neutron scattering [5] from which the various models have been derived. The studies indicate a structure of between 3 and 10 nm in size. More recently experiments have been undertaken using scanning probe microscopy (SPM) [12,13], to study Nafion in differing states of hydration. A number of swelling studies have been carried out on Nafion [14,15] using a wide variety of solvents with some remarkable results, including a swelling of 360% with TBP as used by Lehmani et al. [13] in their SPM study.

Nafion has proved to be a suitable sample for other forms of SPM including scanning tunnelling microscopy (STM) and scanning electrochemical microscopy (SECM) [16,17]. Fan and Bard [16] studied a spin-coated Nafion film using SECM and found a domain-like structure, consisting of circular structures, 1–2 nm in diameter made up from a conductive central zone surrounded by a less conductive region.

Tapping mode phase imaging is a relatively new atomic force microscopy (AFM) [18] technique, it can differentiate between areas with different properties regardless of their topographical nature [19–25]. The phase angle is defined as the phase lag of the cantilever oscillation relative to the signal sent to the piezo-driving the cantilever. Its value depends on the energy dissipated in the tapping interaction of probe and specimen.

Since many of the useful properties of Nafion membranes depend strongly on the water content, studies in different states of hydration might be informative. The difference in probe-specimen adhesion between the hydrophobic backbone and hydrophilic side group regions of the polymer offer the possibility of observing the spatial distribution of these two regions, and therefore test the proposed models through phase imaging.

2. Experimental method

2.1. Sample preparation

The membrane will readily rehydrate if left exposed to a high relative humidity environment. Careless handling can result in the membrane ion-exchanging from the acid (H^+) to a salt form (e.g. Na^+ or K^+). All samples were therefore routinely prepared by refluxing with a 50/50 mixture of concentrated nitric acid and de-ionized water to ensure that the membrane is in the H^+ form and free from any chemical impurities.

Circular samples of one centimetre in diameter were mounted on magnetic stainless steel stubs, placed in the Digital Instruments Extended Multimode AFM and imaged in tapping mode with silicon cantilevers in order to provide topography and corresponding phase images. The membrane and microscope were placed in a purpose built environmental chamber and dehydrated overnight. A variety of techniques were employed to reduce the humidity including silica gel, phosphorus pentoxide, a liquid nitrogen

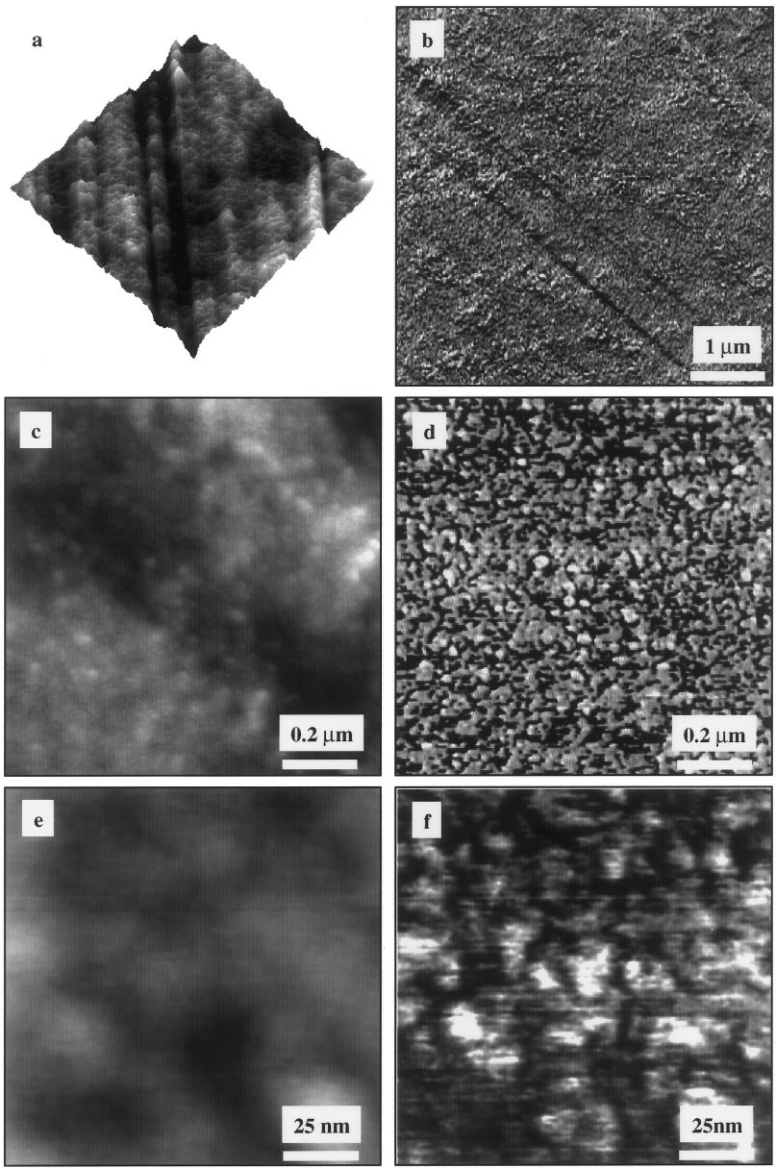

Fig. 2. 5 μm, 1 μm and 125 nm wide topography and corresponding phase images of Nafion 115 imaged under ambient conditions. The *Z* scales are 30, 30 and 10 nm, respectively.

cold finger and dry Nitrogen gas. A humidity minimum of $(0.8 \pm 2.0)\%$ was obtained using Nitrogen gas passed through a molecular sieve. The sample was then imaged and allowed to rehydrate slowly to room humidity (~34%) over the course of 12 h whilst being continuously imaged, and the humidity recorded.

2.2. Image analysis

As the energy loss is proportional to the sine of the phase angle, the phase images from the rehydration sequence were converted to their sine in accordance with Eq. (1). A bearing analysis (Digital Instruments proprietary software) was then performed on these images to determine the percentage of each image at any given sine value and how this changed with humidity. These results are displayed graphically in Fig. 5. The integral under these curves, the phase angle "volume", obtained by effectively multiplying the image area by the sine of the phase angle, is proportional to the total energy dissipated over the whole sample. A plot of phase angle "volume" against humidity is shown in Fig. 6 for all of the images in the re-hydration sequence.

Phase images from the beginning and end of the rehydration sequence were analysed further with the aid of a cluster counting algorithm [26]. The 256×256 images were exported, cropped, saved as eight-bit data and then converted to binary. A series of thresholds from 0 to 256 were then applied to all the data points in the image; if the point was equal to or greater than the threshold value it was set to one, and, if not, it was set to zero. A cluster is defined as two or more touching pixels. The number of unique clusters, total area of clusters and average cluster area was then

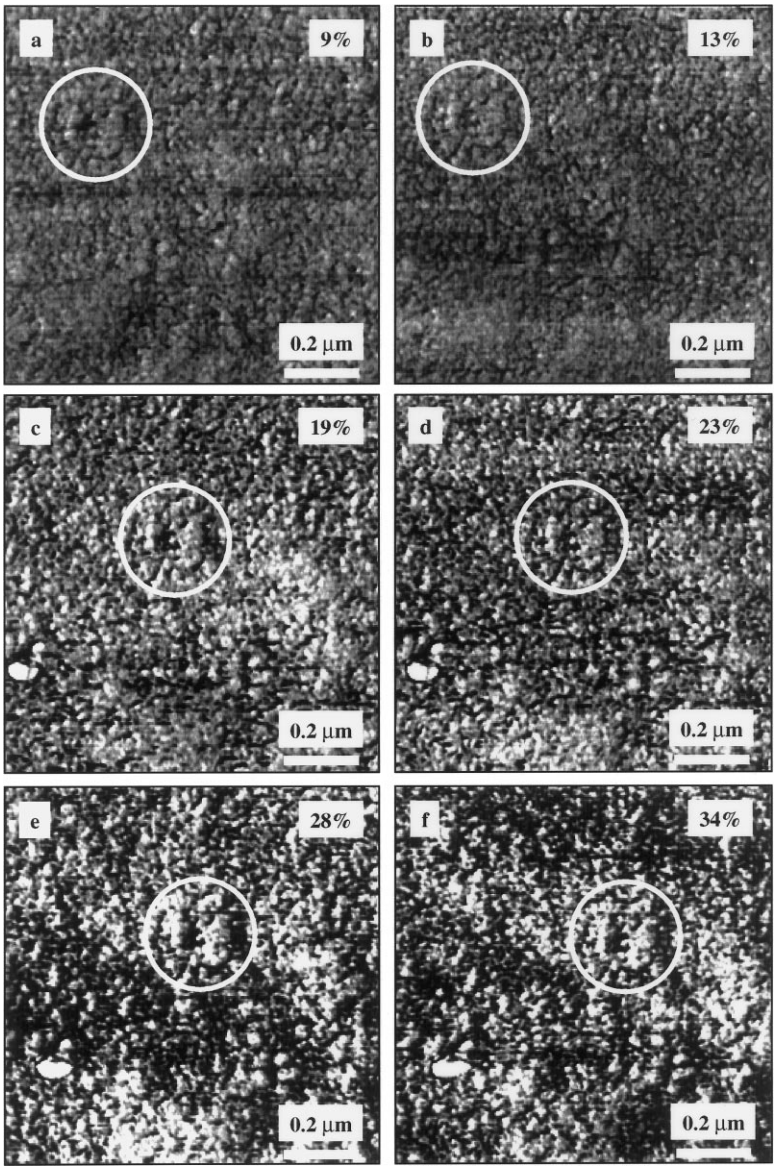

Fig. 3. Six 1 μm wide phase images of the same area of Nafion at a range of humidities between (9 and 34) ± 2%. (*Z* scale = 30°.)

calculated for each threshold. A plot of number of clusters against threshold for the two humidity extremes is shown in Fig. 7.

3. Results and discussion

3.1. Comparison of AFM images to models

Tapping mode topography and the corresponding phase images of 1100 EW Nafion membranes recorded under ambient conditions on three different size scales are shown in Fig. 2. A 5 μm wide three-dimensional topography image and its corresponding phase signal are shown in Fig. 2a and b, respectively. Extrusion marks produced during manufacture of the polymer film can easily be seen running from top to bottom in the height image (Fig. 2a) and less easily from top left to bottom right in the phase image (Fig. 2b).

Features common to all models of Nafion are hydrophilic sulphonic acid-rich regions around which the free and bound water forms conduction pathways. The differences lie in the size and arrangement of the periodic structures responsible for the X-ray patterns from which the models were created. This characteristic spacing is assigned in the case of the Two-Phase Model [5,27] to the ionic cluster spacing, in the Core–Shell model [5,28,29] to the radius of the ion rich-core, and to the inter-lamellar spacing in the Lamellar model [5,30].

A 1 μm wide topography and corresponding phase signal are shown in Fig. 2c and d. Cluster-like structures as proposed in the Two-Phase Model [5] become clearly

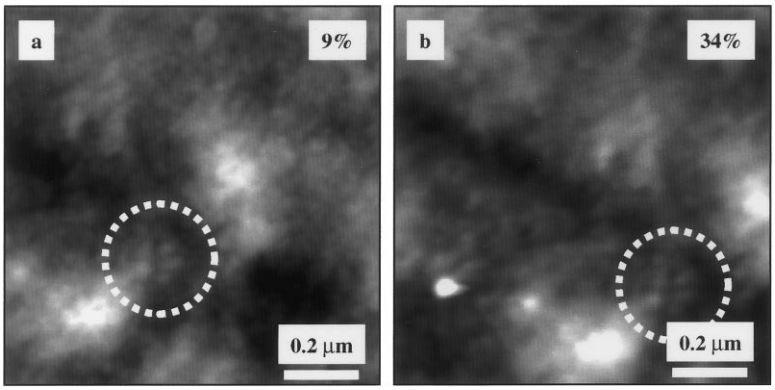

Fig. 4. Corresponding topography images for the humidity extremes of (9 and 34) ± 2%. (*Z* scale = 50 nm.)

visible in the phase signal. These structures do not always correspond to features in the height image. Features at the same height can have a different phase signal and visa versa, indicating minimal topographic coupling. A high resolution, 125 nm topography and phase image pair is shown in Fig. 2e and f. Cluster-like structures with a diameter of 5–30 nm are clearly visible, particularly in the phase image, this is consistent with earlier AFM studies.

Samples produced by evaporating a dilute solution of Nafion on to gold-sputtered cover slips were found to have a fibril network structure, which became more ordered as the membrane swelled [12]. Commercially available 1100 EW Nafion 117 was dehydrated in a vacuum oven at 80°C and was first imaged "dry", then swollen with de-ionized water, and finally swollen with tributylphosphate (TBP) [13]. A super-structure of spherical domains with an average diameter of 45 nm containing 11 nm grains was found. According to the section analysis of the microstructure, the interstitial regions have a mean thickness of 5 nm, which may correspond to the cluster size.

3.2. Water absorption

The effect of water absorption is different in each of the models. In the Two-Phase and Core–Shell models the water is taken up spherically, so the lateral swelling should be proportional to the cube root of the volume fraction of water absorbed. While in the Lamellar model the swelling

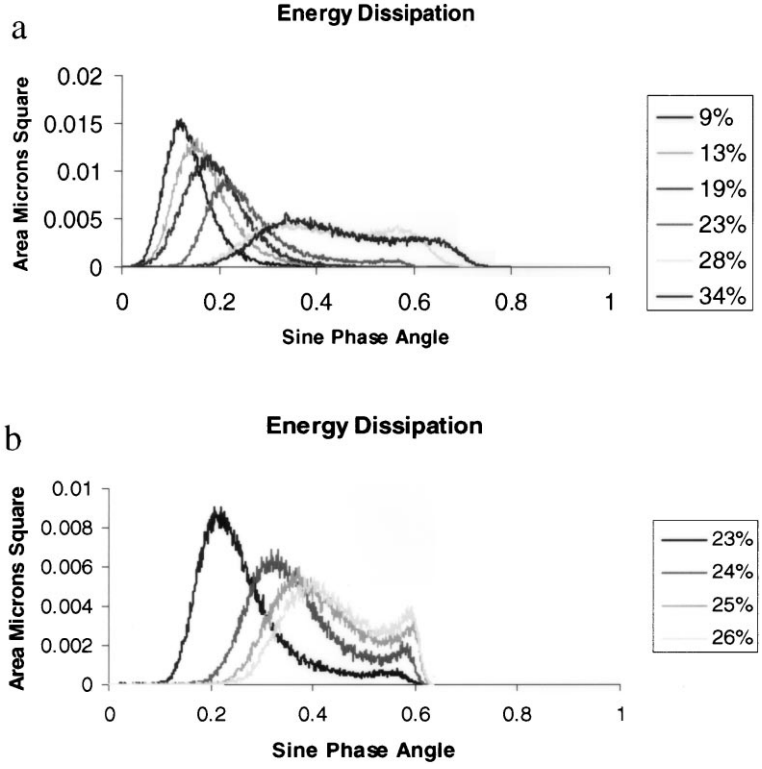

Fig. 5. A graph of area vs. Sine (phase angle) demonstrating how the energy dissipated over the sample varies with humidity.

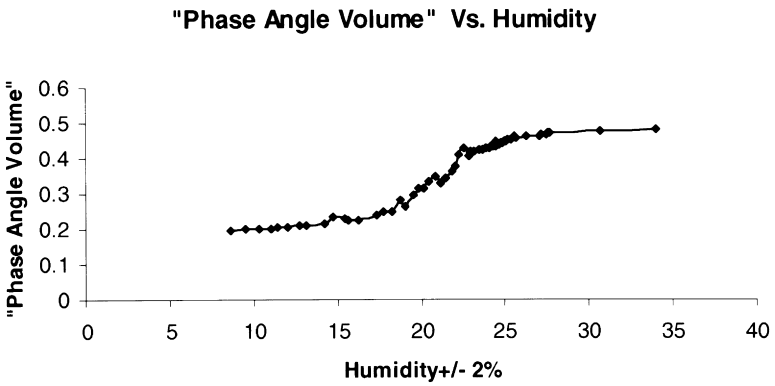

Fig. 6. A graph of "phase angle volume" against humidity.

is treated one-dimensionally and the expansion is directly proportional to the volume fraction of water absorbed. The Cluster-Network model [5,31] postulates a large-scale organisation of clusters with transient connective tubes which are in constant flux. A fully reversible dynamic reorganisation of the clusters is proposed to occur on rehydration. Positron annihilation spectroscopy has also been used to study different cation forms of Nafion membranes by measuring the free volume. These studies [32,33] found that the formation and expansion of clusters is always associated with a change in free-volume structure resulting in smaller free-volume holes.

Six 1 μm wide phase images from a sequence of 56 images of 1100 EW Nafion obtained over a range of humidities from (9–34) ± 2% are shown in Fig. 3a–f. The phase image contrast increases with humidity as the hydrophilic sulphonic acid groups incorporate water and become more easily distinguished from the hydrophobic regions. It is very difficult to monitor the same area as the membrane expands both vertically and laterally. The same feature has been circled in each of the images to aid comparison and to illustrate the drift to the right, which occurred throughout the series.

The corresponding topography images from the beginning and end of the rehydration sequence is shown in Fig. 4a and b, respectively. The same area has been circled in both images demonstrating the ability to image the same area whilst following a dynamic process. There is no appreciable change between the two images, therefore any topographic coupling in the phase images remains constant and is not responsible for the increase in phase contrast.

3.3. Energy loss interpretation of phase data

Whilst phase imaging is still the subject of much research, there is a consensus that the phase signal change is due to energy loss. The energy loss E_{DIS} has been shown to be proportional to the sine of the phase angle by the following equation [34,35]

$$\sin\psi = \left(\frac{\omega}{\omega_0}\frac{A}{A_0}\right) + \frac{QE_{DIS}}{\pi kAA_0}, \quad (1)$$

where ψ = Phase angle, ω/ω_0 = (working frequency/resonance frequency), A/A_0 = (set point amplitude/free amplitude), Q = quality factor and k = cantilever spring constant.

The sine phase image data sets in Fig. 3 are represented graphically in Fig. 5a, where the area at each given sine Ψ is plotted against the sine of the phase angle for a range of humidities. At lower humidities there is a single well-defined peak, which then broadens asymmetrically and moves to higher values of sine Ψ and therefore higher energy losses with increasing humidity. At higher humidities a second peak appears, at larger energy losses as shown in Fig. 5b.

The sharpness of the first peak indicates that the variation in energy dissipation's at lower humidities is quite small and the surface is approximately homogeneous, while the shift to higher energy losses indicates that there is a bulk change across the sample. The asymmetric broadening of the peak indicates that there is a greater range of energy losses at higher humidities. The appearance of the second peak at higher energy losses indicates that there are two distinct regions with characteristic energy losses within the images above humidities of (23 ± 2)%.

The energy loss could be due one of the two mechanisms; either a viscoelastic or adhesive energy loss. The mechanisms for increasing energy loss with humidity would be, softening of the material due to water absorption in the viscoelastic case or a more adherent surface due to increased water adsorption in the adhesive case. The increased phase contrast between the hydrophobic and hydrophilic regions can easily be explained by the preferential sorption of water to the hydrophilic areas. The elastic response of polymers increases with frequency as shown in the case of Nafion [36], at the frequencies at which the cantilever is being driven ~250 kHz, the viscoelastic energy loss would be negligible and the energy loss mechanism will be primarily adhesive.

The area under the curves, or phase angle volume, in Fig. 5 is proportional to the total energy dissipated over the whole sample. A graph of phase angle volume against humidity has been plotted in Fig. 6. The total energy loss monotonically increases with humidity, with two linear

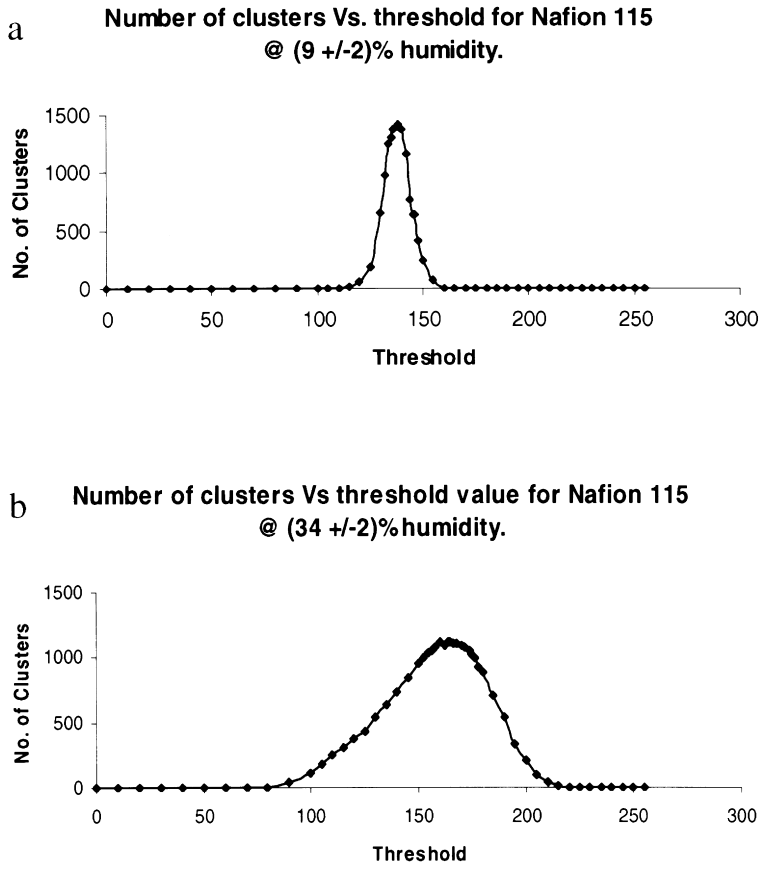

Fig. 7. A graph of number of clusters against threshold value for the two humidity extremes.

regions either side of an apparent transition between (20–25) ± 2% humidity caused by the high energy tail and second energy loss peak appearing in Fig. 5. The typical values below are inserted into Eq. (1) in order to convert the phase angle volume into an actual energy loss

ω/ω_0 = (working frequency/resonance frequency) ~1, A/A_0 = (set point amplitude/free amplitude) ~0.5, Q = (quality factor) ~400 and k = (cantilever spring constant) ~40 N/m.

This gives a typical value of ~3 kJ m^{-2} or 3 nJ μm^{-2}.

3.4. Cluster analysis of phase data

Analysis of the phase images from the beginning and end of the rehydration sequence, with the cluster counting algorithm, are shown in Fig. 7a and b, respectively, and in Table 1.

Table 1
The number of clusters, total percentage area of cluster and average cluster size for 1 μm wide phase images of Nafion at (9 and 34) ±2% humidity

Humidity ±2%	9	34
Number of clusters	1415	1118
Total percentage cluster area	18.9	17.6
Average cluster area (nm^2)	134	158

The sharp peak in Fig. 7a implies that all the clusters have a similar phase angle and therefore energy loss at lower humidities. At higher humidities as shown in Fig. 7b, the peak has moved to higher thresholds as the average energy loss has increased, the peak has also broadened significantly as the clusters have a wider range of energy losses. This broadening of the peak probably explains why the total percentage area of clusters actually decreases with humidity, contrary to what one would expect as lower energy clusters or parts of clusters are no longer counted at higher threshold values. The average cluster area between 134 and 158 nm^2 is consistent with the images shown in Fig. 2, where clusters have a range of sizes between 5 and 30 nm (or approximate areas of 25–900 nm^2). This is significantly larger than the ~4 nm structures proposed from X-ray studies [6–9], probably due to the formation of cluster agglomerates. The decreasing number of clusters and corresponding increase in average cluster size with humidity is consistent with recent X-ray diffraction results [37,38] and implies a cluster rearrangement similar to that proposed by Hsu and Gierke [31]. The percentage of the surface covered by clusters at 34 and 9% humidities, is 17.6 and 18.9%, respectively. This is considerably larger than a value of 7.6%, calculated assuming: that the membrane is homogeneous and dry, that the mass of SO_3H to be 81.1 g and the equivalent weight of the membrane to be 1070

((81.1/1070) × 100). However, the membrane is not dry and will have incorporated water preferentially into the hydrophilic clusters which will have swollen, the surface may not be representative of the bulk and the sulphonic acid groups are 8% by mass but not necessarily by volume.

4. Conclusions

Tapping mode phase imaging was successfully used to identify the hydrophobic and hydrophilic regions of Nafion perfluoro-sulphonate cation exchange membranes. Since there is often little correlation between the topography and phase images, it is a useful tool for identifying and mapping regions with different properties, irrespective of their topographical nature. The images support a cluster model for Nafion at humidities in the range (9–34) ± 2%. The clusters have a range of sizes from 5 to 30 nm, significantly larger than the ~4 nm structures proposed from X-ray studies, this is probably due to the formation of cluster agglomerates.

Phase images can now be interpreted more quantitatively in terms of energy loss, an algorithm converting the phase signal to its sine has been written allowing an investigation of energy loss over a sample, typically giving values in the order of $3\,kJ\,m^{-2}$. The main energy loss mechanism is believed to be adhesive rather than viscoelastic. The energy loss increased with humidity and it became easier to distinguish between the hydrophobic and hydrophilic regions, which displayed characteristic energy losses. A cluster counting program has also been written to ascertain the number and size of features, when applied to phase images of Nafion perfluorosulphonate membranes, the number of clusters decreased and the average cluster size increased with increasing humidity. The percentage area of clusters on the surface under ambient conditions ~18% was considerably larger than that the ~8% predicted for a homogeneous dry membrane.

Acknowledgements

The authors would like to thank Massimo Antognozzi, James Elliott and James Wescott for their assistance with the computer programming. This work was financially supported by the EPSRC and National Power PLC.

References

[1] Yeager HL, Steck A. Cation and water diffusion in Nafion ion exchange membranes: influence of polymer structure. J Electrochem Soc 1981;128:1880–4.
[2] Yeager HL, O'Dell B, Twardowski Z. Transport properties of Nafion membranes in concentrated solution environments. J Electrochem Soc 1982;129:85–9.
[3] Tant MR, Mauritz KA, Wilkes GL. Ionomers: synthesis, structure, properties and applications, London: Chapman & Hall, 1997.
[4] Zawodzinski TA, Springer TE, Davey J, Jestel R, Lopez C, Valerio J, Gottesfeld S. A comparative-study of water-uptake by and transport through ionomeric fuel-cell membranes. J Electrochem Soc 1993;140:1981–5.
[5] Eisenberg A, Yeager HL. Perfluorinated ionomer membranes, Washington, DC: ACS Books, 1982.
[6] Gierke TD, Munn GE, Wilson FC. The morphology in Nafion perfluorinated membrane products, as determined by wide-angle and small-angle X-ray studies. J Polym Sci 1981;19:1687–704.
[7] Roche EJ, Pineri M, Duplessix R, Levelut AM. Small-angle scattering studies of Nafion membranes. J Polym Sci 1981;19:1–11.
[8] Fujimura M, Hashimoto T, Kawai H. Small-angle X-ray-scattering study of perfluorinated ionomer membranes. 1. Origin of 2 scattering maxima. Macromolecules 1981;14:1309–15.
[9] Fujimura M, Hashimoto T, Kawai H. Small-angle X-ray-scattering study of perfluorinated ionomer membranes. 2. Models for ionic scattering maximum. Macromolecules 1982;15:136–44.
[10] Rieberer S, Norian KH. Analytical electron-microscopy of Nafion ion-exchange membranes. Ultramicroscopy 1992;41:225–33.
[11] Porat Z, Fryer JR, Huxham M, Rubinstein I. Electron-microscopy investigation of the microstructure of Nafion films. J Phys Chem 1995;99:4667–71.
[12] Chomakova-Haefke M, Nyffenegger R, Schmidt E. Structure reorganisation in polymer films of Nafion due to swelling studied by scanning force microscopy. Appl Phys A 1994;59:151–3.
[13] Lehmani A, Durand-Vidal S, Turq P. Surface morphology of Nafion 117 membrane by tapping mode atomic force microscopy. J Appl Polym Sci 1998;68:503–8.
[14] McCain GH, Covitch MJ. Solubility characteristics of perfluorinated polymers with sulfonyl fluoride functionality. J Electrochem Soc 1984;131:1350–2.
[15] Gebel G, Aldebert P, Pineri M. Swelling study of perfluorosulphonated ionomer membranes. Polymer 1993;34:333–9.
[16] Fan FF, Bard AJ. STM on wet insulators: electrochemistry or tunneling? Science 1995;270:1849–52.
[17] Mirkin MV. Recent advances in scanning electrochemical microscopy. Anal Chem News Features A 1996;68:177–83.
[18] Binnig G, Quate CF, Gerber C. Atomic force microscope. Phys Rev Lett 1986;56:930–3.
[19] Babcock KL, Prater CB. Phase imaging—beyond topography. 1995, D.I. Application Note A12.
[20] Whangbo MH, Magonov SN, Bengel H. Tip-sample force interactions and surface stiffness in scanning probe microscopy. Probe Microscopy 1997;1:23–42.
[21] McMaster TJ, Hobbs JK, Barham PJ, Miles MJ. AFM study of in situ real time polymer crystallization and spherulite structure. Probe Microscopy 1997;1:43–56.
[22] Tamayo J, Garcia R. Deformation, contact time and phase contrast in tapping mode scanning force microscopy. Langmuir 1996;12:4431–5.
[23] Leclere P, Lazzaroni R, Bredas JL, Yu JM, Dubois P, Jerome R. Microdomain morphology analysis of block copolymers by atomic force microscopy with phase detection imaging. Langmuir 1996;12:4317–9.
[24] Howard AJ, Rye RR, Houston JE. Nanomechanical basis for imaging soft materials with tapping mode atomic force microscopy. J Appl Phys 1996;79:1885–90.
[25] Tamayo J, Garcia R. Effects of elastic and inelastic interactions on phase contrast images in tapping-mode scanning force microscopy. Appl Phys Lett 1997;71:2394–6.
[26] Elliott JA. 1998. Personal communication.
[27] Marx CL, Caulfield DF, Cooper SL. Morphology of ionomers. Macromolecules 1973;6:344–53.
[28] Macknight WJ, Taggart WP, Stein RS. A model for the structure of ionomers. J Polym Sci C 1974;45:113–28.
[29] Kao J, Stein RS, Macknight WJ, Taggart WP, Cargill GS. Structure of the cesium salt of an ethylene–methacrylic acid copolymer from its radial distribution function. Marcomolecules 1974;7:95–100.

[30] Roche EJ, Stein RS, Russell TP, Macknight WJ. Small-angle X-ray scattering of ionomer deformation. J Polym Sci, Polym Phys Ed 1980;18:1497.
[31] Hsu WY, Gierke TD. Ion-transport and clustering in Nafion perfluorinated membranes. J Membrane Sci 1983;13:307–26.
[32] Sodaye HS, Pujari PK, Goswami SB, Manohar SB. Probing the microstructure of Nafion-117 using positron annihilation spectroscopy. J Polym Sci B 1997;35:771–6.
[33] Sodaye HS, Pujari PK, Goswami SB, Manohar SB. Measurement of free-volume hole size distribution in Nafion-117 using positron annihilation spectroscopy. J Polym Sci B 1998;36:983–9.
[34] Cleveland JP, Anczykowski B, Schmid AE, Elings VB. Measuring energy dissipation with a tapping-mode atomic force microscope. Appl Phys Lett 1998;72:2613–5.
[35] Tamayo J, Garcia R. Relationship between phase shift and energy dissipation in tapping-mode scanning force microscopy. Appl Phys Lett 1998;73:2926–8.
[36] Eisenberg A, King M. Ion-containing polymers, Physical properties and structure, 2. London: Academic Press, 1977 p. 164.
[37] Elliott JA. PhD thesis, X-ray diffraction and computer modelling of perfluorinated ionomer membranes, 1998.
[38] Elliott JA, Hanna S, Elliott AMS, Cooley GE. Interpretation of the small-angle X-ray scattering from swollen and oriented perfluorinated ionomer membranes. Macromolecules 1999 (submitted).